Int J Clin Exp Pathol 2018;11(3):1273-1280
www.ijcep.com /ISSN:1936-2625/IJCEP0071276

Original Article

In vivo evaluation of bronchial injury of irreversible electroporation in a porcine lung ablation model by using laboratory, pathological, and CT findings

Jun-Hui Sun[1,2,3,4], Tong-Yin Zhu[1,2,3,4], Xin-Hua Chen[1,2,3,4], Chun-Hui Nie[1,2,3,4], Zhi-Gang Ren[5], Guan-Hui Zhou[1,2,3,4], Tan-Yang Zhou[1,2,3,4], Sheng-Yong Yin[1,2,3,4], Zhi-Yi Peng[1,2,3,4], Li-Ming Wu[1,2,3,4], Xiong-Xin Zhang[2,3,4], Wei-Lin Wang[1,2,3,4], Shu-Sen Zheng[1,4]

[1]Hepatobiliary and Pancreatic Interventional Treatment Center, Division of Hepatobiliary and Pancreatic Surgery, The First Affiliated Hospital, School of Medicine, Zhejiang University, Hangzhou, China; [2]Key Laboratory of Precision Diagnosis and Treatment for Hepatobiliary and Pancreatic Tumor of Zhejiang Province, Hangzhou, China; [3]Clinical Medical Research Center for Hepatobiliary and Pancreatic Disease of Zhejiang Province, Hangzhou, China; [4]Key Laboratory of Combined Multi-organ Transplantation, Ministry of Public Health, Hangzhou, China; 5Department of Infectious Diseases; Precision Medicine Center, The First Affiliated Hospital of Zhengzhou University, Zhengzhou, China

Received December 20, 2017; Accepted January 12, 2018; Epub March 1, 2018; Published March 15, 2018

Abstract: Irreversible electroporation (IRE) creates permanent pores in the cell membrane, leading to irreversible cell death. In this study, the impact of IRE on bronchial injury was comprehensively examined in a timed series study. Altogether, 8 Bama miniature pigs were included in this study and were randomly assigned to experimental and control groups. The experimental group underwent IRE that was guided and monitored by spiral computed tomography (CT). The monopole probe of the IRE was positioned at the right pulmonary hilum. Specimens were collected at 0 h, 2 h, 2 d, 7 d, and 14 d after the IRE procedure for a pathological examination. A small amount of needle-tract bleeding occurred in two animals, and mild pneumothorax occurred in another. IRE can elicit acute bronchial inflammation, bleeding, and mucosal injury, but severe complications were not found. Pathological examinations and transmission electron microscopy (TEM) showed dead vascular epithelium cells in the region of the ablation, while the bronchioli and the vascular extracellular matrix were preserved. At 2 hours post-IRE, there were marked increases in bronchoalveolar macrophages ($P<0.001$), but the inflammation could recover after 14 days and showed no statistical significance when compared with the control group at the same time. In conclusion, CT-guided IRE ablation can elicit acute but recoverable bronchial inflammation, bleeding, and mucosal injury in porcine lung tissues. However, longer follow-up is still required to establish an evaluation of the long-term safety.

Keywords: Lung ablation, irreversible electroporation, computed tomography (CT), bronchial injury, porcine model, transmission electron microscopy (TEM)

Introduction

Lung carcinoma is one of the most common malignant tumors worldwide. With a more rapidly increasing rate than in Western countries, lung carcinoma in China has been at the top in terms of cancer diagnosis and cause of cancer-related death for many years. In addition to surgery, local thermal ablation has been widely used as a treatment strategy. Radiofrequency ablation is the most commonly used approach, while microwave ablation, cryoablation and laser ablation are also applied extensively [1-5]. However, these heating or freezing-based modalities are associated with potential damage to collateral tissues. Importantly, treatment of central lung cancer using such techniques is limited by the possible damage to the blood vessels and bronchi of the hilar region. Furthermore, the complete efficacy of thermal ablation can be limited by the influence of the heat-sink effect from large vessels [1, 2]. As a non-thermal, minimally invasive ablation technique, irreversible electroporation (IRE) could

be used to treat patients with lung tumors that are located close to the chest wall and that are not suitable for surgery [6]. This technique delivers electrical pulses with a short duration (microsecond) and high voltage directly to the targeted tissue. IRE generates irreversible perforations in the phospholipid bilayer on the cell membrane, leading to cell death. However, the vascular system, which is rich in colloids, is preserved [7-9]. Although the actual mechanism of IRE ablation remains to be fully elucidated, it is generally accepted that the effects of IRE are mediated by the induction of apoptosis, whereas proteins are unaffected and vascular and collagenous structures are left intact, since IRE has the advantage of tissue selectivity. Currently, this technique is available through NanoKnife (NanoKnife, AngioDynamics, Latham, NY) [10], making the standard implementation of IRE ablation possible. Clinical trials of IRE ablation have shown that IRE is effective in liver carcinoma [11-13], pancreatic carcinoma [13, 14], prostate carcinoma [13, 15] and renal cell carcinoma [16]. However, satisfactory effects of IRE technology have not yet been achieved in lung carcinoma [17-19]. Therefore, further animal studies using NanoKnife IRE ablation on the porcine lung are still needed to rationalize the procedure, and parameters [20-22]. Our current study is focused on looking at bronchial injury comprehensively using a serial follow up. Computed tomography (CT) is the most commonly used image-guidance method of lung puncture. Therefore, CT guidance was used in this study to perform the percutaneous IRE ablation on porcine lung tissues and post-IRE ablation follow-up. Animals were closely observed for the occurrence of postoperative complications, as well as serial laboratory exams on bronchial injury and infection, including myocardial enzymes, leukocyte counts, and pathological changes after the IRE ablation.

Materials and methods

Experimental animals

All animal experiments were approved by the Animal Care and Use Committee of Zhejiang University Medicine School (China). A total of eight adult Bama miniature animals (female; mean weight, 25 ± 3.23 kg, purchased from Shanghai Jambo Biological Technology Co., Ltd, Shanghai, China) were enrolled in this study. All animals were maintained in the Laboratory of Animal Center of Zhejiang University Medicine School. Appropriate handling and care was provided by trained staff and a licensed veterinarian. The animal operations were performed in accordance with the principles of the Animal Center of Zhejiang University Medicine School guidelines.

The IRE apparatus

The NanoKnife Ablation System (NanoKnife, AngioDynamics, Latham, NY, USA), was used for the ablation of porcine lung tissues [25]. The ablation system includes a pulse generator, a pair of ablation probes, and an ECG synchronization device. The two monopole probes (diameter, 19-G; length, 15 cm) were used for ablation. The probe tip was adjustable from 0-4 cm. The same puncture length of the electrode was set at 2 cm in this study for ease of comparison. The standard treatment protocol was set up according to the manufacturer's manual. A series of 90 pulses were released. The pulse generator was triggered by R waves, which were detected automatically by ECG. The generator produced the electrical pulses with a time delay of 50 ms, and this time-point was during the ventricular refractory period. The probes were placed under the guidance of a 256-slice CT scanner (Brilliance iCT, Philips), with a scanning voltage of 120 kV. The scanning slice thickness and gap were both set at 5 mm.

CT-guided IRE procedure

The Bama miniature pigs were numbered from 1 to 8 and assigned randomly to the experimental group (n=6) and the control group (n=2) [21, 26]. Ablation was performed after a 12 h period of fasting and a 6 h period of water deprivation. Indwelling needles penetrated the auricular veins and venous transfusions were established. Anesthesia was induced by the intravenous injection of rocuronium 0.6 mg/kg and was sustained by the administration of propofol 5 mg/(kg·h) and rocuronium 0.15 mg/(kg·h). After endotracheal intubation, the animals were connected to a mechanical ventilator. Heart rate and respiration were closely monitored by an ECG. The right lateral thoracic wall was sterilized in preparation for the surgical procedure. The animals were placed in the left lateral decubitus position on the CT scan

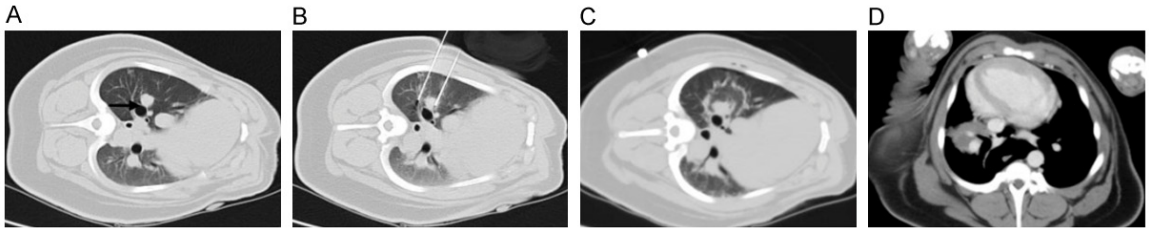

Figure 1. CT-guided NanoKnife knife ablation process. A. The right pulmonary hilum (indicated by the arrow) was selected as the target region for ablation. B. Two 19-G monopole ablation probes were inserted parallel to the bilateralis of the target region. C. CT scanning performed immediately after ablation. D. Enhanced CT scanning performed 24 h after the ablation (n=6).

table. The metal positioning grid was placed on the skin's surface. The right pulmonary hilum was regarded as the target region for ablation. The needle puncture path was designed to avoid anatomical structures such as the ribs, vessels and interlobular fissure. The operator was required to choose the shortest possible pathway. The puncture point at the surface was detected and marked. After routine disinfection and application of sterile drapes, an incision (length 2 mm) was made at the puncture site using a razor blade due to the toughness of the animal's skin. Under CT guidance, two ablation probes were inserted to a depth that reached the ablation region via a route that was parallel to the predetermined pathway. The intervals between the probes ranged from 1.2 to 2.0 cm. Test electrical impulses were administered in order to observe the conditions of the muscle contractions. After confirming that the electrical impedance of the organization was in the acceptable range, the ablation was carried out. After the completion of the ablation, the probes were removed, and the animal underwent another spiral CT scan to confirm the absence of complications in the hemothorax, pulmonary hemorrhage and severe pneumothorax. At the end of the procedure, the puncture site was disinfected and covered with the applicator. The animals were covered with blankets and housed in a warm environment. Mechanical ventilation was continued until the recovery of spontaneous breathing and free movement in the animals. The animals were then returned to the Laboratory Animal Center of Zhejiang University Medicine School, where they received food and water regularly and their post-operative conditions were observed. The surgical procedures were aseptic and the animals retained an intact immune system. Therefore, the breeding conditions were set to the clean level and antibiotics were not administered to prevent infections. All of the animals underwent contrast-enhanced CT scanning 24 h after the surgery.

Post-IRE ablation follow-up

The following parameters were monitored: (1) intra-operative and post-operative complications; (2) biochemical tests of blood samples that were collected before surgery (baseline) and at 2 h, 2 d,7 d, and 14 d after the operation; white blood cell counts were detected using flow cytometry; serum levels of aspartate aminotransferase (AST), lactate dehydrogenase (LDH), creatine kinase MB (CKMB), hydroxybutyrate dehydrogenase (HBD) and were detected by nephelometry; (3) pathology examinations were performed on the animals that were randomly selected for euthanization (air embolism method) at 2 h (n=1), 2 d (n=2), 7d (n=2) and 14 d (n=1) after the surgery. The lung tissues of the ablation regions were obtained and fixed by immersion in a 10% formalin solution. Pathological sections were prepared (10 μm) and the results of hematoxylin and eosin (H&E) staining were observed under a microscope (LEICA, model: DMLB). The conditions of tissue necrosis and repair were observed. The animals in the control group were randomly selected and euthanized in parallel, and pathological sections were prepared as blank controls.

A pathological study using an H&E stain and TEM was performed on the 14th day post IRE ablation; the animals were euthanized and the specimens were fixed with paraformaldehyde and glutaraldehyde, respectively. The ultrastructural changes were observed using an H&E stain and SEM. The lung samples were

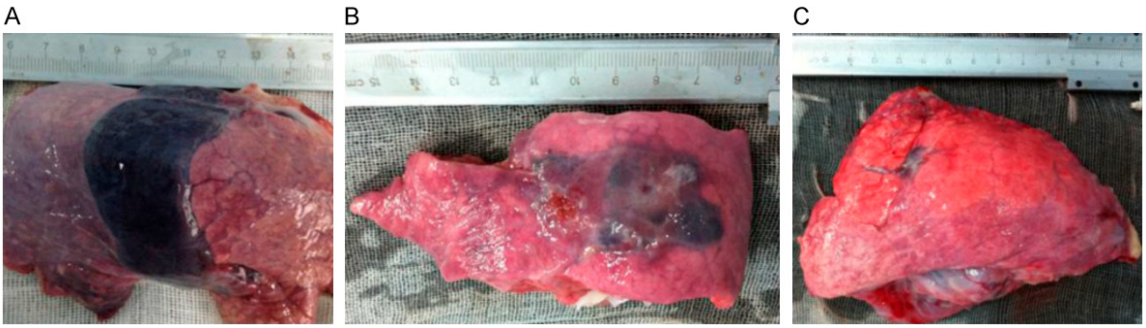

Figure 2. Gross anatomy of the lungs after the ablation. A. 2 days after ablation (n=2). B. 7 days after ablation (n=2). C. 14 days after ablation (n=1).

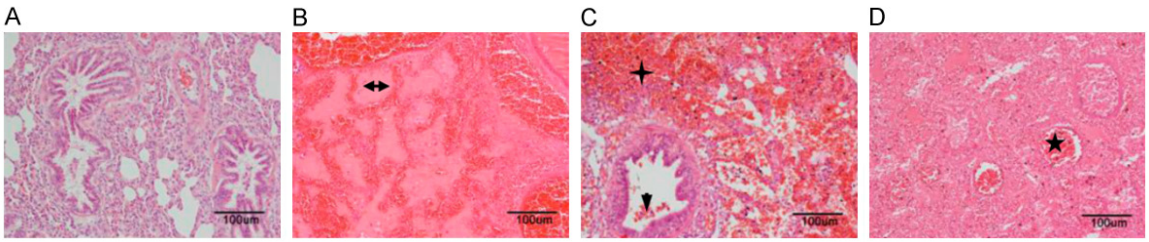

Figure 3. Pathological changes in the lung tissue after ablation. HE staining (200× magnification). A. Lung tissues in the control group (n=2). B. At 2 days after ablation, hemoglobin and collagen (horizontal arrow) were present in the alveoli and bronchioles of the ablation regions (n=2). C. At 7 days after ablation, dead vascular endothelial cell debris (downward arrow), hemoglobin (cross), and infiltrating macrophages were present in the alveoli and bronchioles of the ablation region (n=2). D. At 14 days after ablation, gradual regeneration of the alveoli, bronchioles and vascular endothelial cells was observed, although the inner cavities (star) were still occluded (n=1).

fixed in 2.5% glutaraldehyde at 4°C overnight and then in 2% OsO4 for 24 hours, followed by dehydration in a series of ethanol. After coating the samples with gold, pictures were taken of the samples in the Electron Microscopic Center of Zhejiang University. The lung samples were fixed in 10% formalin and then embedded in paraffin, cut into 5-μm slide sections, and stained with hematoxylin and eosin (H&E), and pictures were taken under light microscopy to evaluate tissue structure and pathological changes.

Results

The results of the CT scan identified the well-defined ablation zone with sharp margins after IRE ablation. Under CT-guidance, the most dangerous anatomy for the traditional thermal ablation, the right pulmonary hilum, was selected as the ablation target (**Figure 1A**). Two 19-G monopole ablation probes were inserted parallel to the bilateralis region (**Figure 1B**). CT scanning immediately after the NanoKnife ablation revealed the rectangular areas of ground-glass opacity in the ablation region, with serrated edges of high density (**Figure 1C**). Enhanced CT scanning performed 24 h after ablation showed significantly increased density in the area of the ablation. Notably, the lower right pulmonary artery, vein, and bronchus remained unobstructed (**Figure 1D**). Complete ablation of the target region was successfully achieved in all of the animals. The intraoperative anesthesia kept the animals stable, and no obvious arrhythmias, such as ventricular tachycardia and atrial fibrillation, occurred. Needle-tract bleeding was found in two cases, and one case showed symptoms of mild pneumothorax so no special treatment was administered and no hemopneumothorax was found. All of the experimental animals had achieved post-anesthesia recovery 0.5 to 2 h post IRE and then resumed their regular activities and food intake. IRE caused full destruction in the ablation zone marked by gross anatomy. The lungs of the experimental animals were removed at specific time-points after ablation. Inspection of the

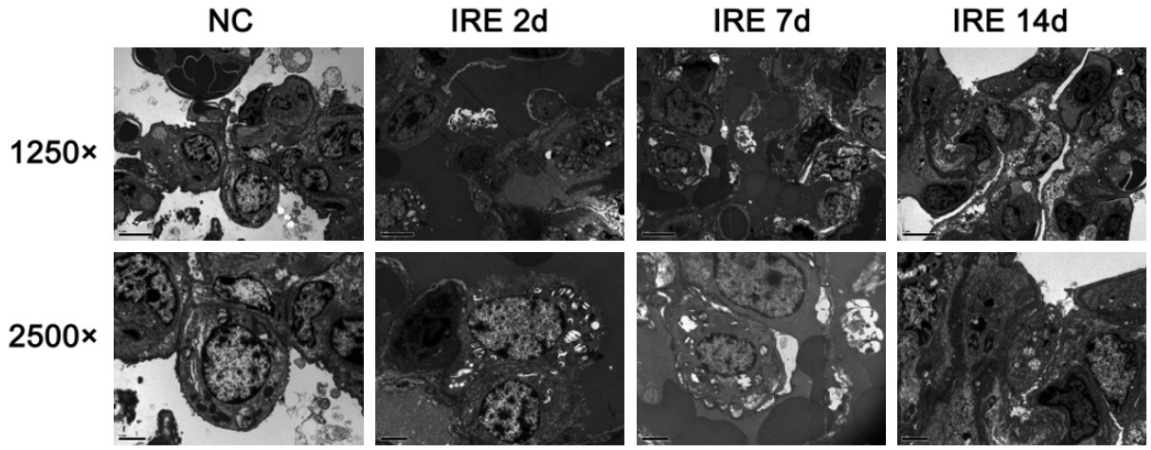

Figure 4. IRE caused the ultrastructure changes of the lung by TEM. The ultrastructure changes of the lung presented using a transmission electron microscope at 2, 7, and 14 days after IRE ablation. The magnification in the upper panel is 1250 and the magnification in the lower panel is 2500.

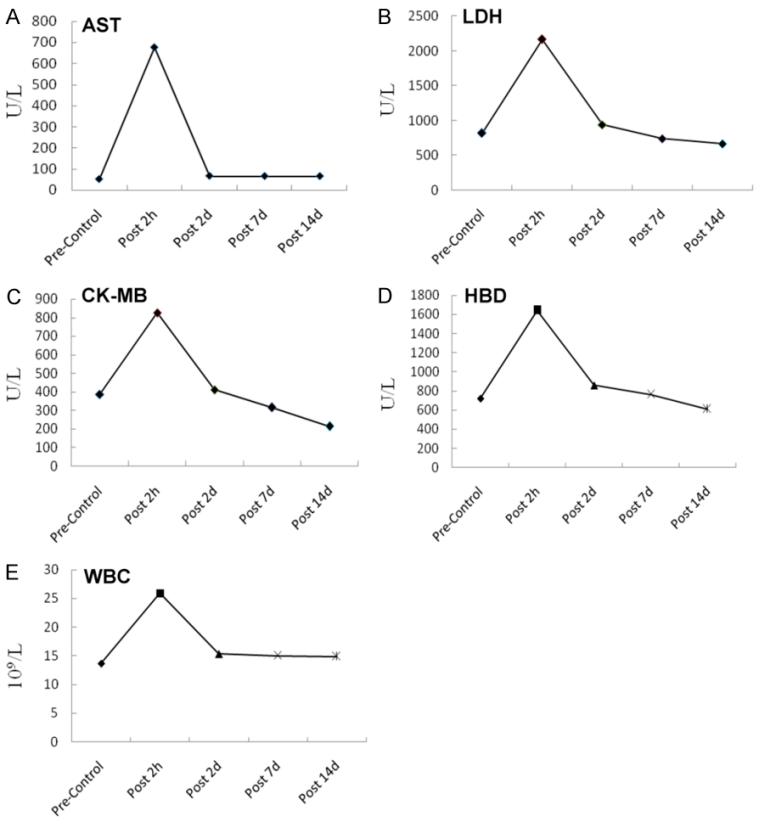

Figure 5. Biochemical and WBC changes in the lungs after ablation. Serum levels of biochemical markers were determined by nephelometry. A. Aspartate aminotransferase (AST). B. Lactate dehydrogenase (LDH). C. Creatine kinase MB (CK-MB). D. Hydroxybutyratedehydrogenase (HBD). E. White blood cells (WBC) were analyzed using flow cytometry. (Pre-Control: n=8, Post 2 h: n=6, Post 2 d: n=5, Post 7 d: n=3, Post 14 d: n=1).

gross anatomy of the lungs at 2 days after ablation revealed clear boundaries between the darkened tissues in the ablation region and the surrounding normal lung tissues (**Figure 2A**). At 7 days after the ablation, the color of the lung tissues in the ablation region had faded and the size of the ablation region had decreased when compared with the control group at the same time point (**Figure 2B**). At 14 days after the ablation, the ablation area of the lung tissues was considerably reduced (**Figure 2C**). IRE caused the bronchial injury marked by pathology. Compared with the control group (**Figure 3A**), H&E staining of the lung tissue sections 2 days after the ablation showed that injured vascular endothelial cell debris, hemoglobin, and infiltrating macrophages were present in the alveoli and bronchioles of the ablation region (**Figure 3B**). At 7 days after the ablation, hemoglobin and collagen were still present in the alveoli and bronchioles of the ablation regions (**Figure 3C**). At 14 days after the ablation, gradual regeneration of the alveoli, bronchioles and vascular endothelial cells was observed, although the inner cavities were still

occluded (**Figure 3D**). IRE caused ultrastructure changes of the lung marked by TEM at 2 days after IRE ablation, and the apical surface of epithelial cells was disrupted, leading to narrowed and contracted bronchial lumen. At 7 days post-IRE, the recovery phase occurred. The injured epithelial cell membranes were restored to their organized assembly on the underlying smooth muscle cells. At 14 days post-IRE, the previously stretched epithelial and smooth muscle cells lined up orderly in the bronchial lumen with fine cilia (**Figure 4**). IRE caused acute inflammation, marked by biochemicals and White Blood Cell (WBC). Two hours after ablation, the serum levels of Aminotransferase (AST), Lacrate Dehydrogenase (LDH), Creatine Kinase-Myocardial Isoenzyme (CKMB), and Hydroxy butyrate Dehydrogenase (HBD) were significantly increased and were three times higher than those of the preoperative levels (pre-control) (**Figure 5A-D**). At 2 days after ablation, the levels of these indicators had returned to their pre-operative baseline. Furthermore, at 2 h after ablation, the WBC count significantly increased, with numbers approximately 2-fold greater than those observed pre-operatively (**Figure 5E**). At 2 days after ablation, the WBC count had returned to the pre-operative level, with no further elevations in the counts observed at the later time-points. This observation indicates that the transient elevation in WBC numbers may be caused by a stress response, rather than by infection.

Discussion

In this study, we assessed bronchial injury caused by percutaneous IRE ablation of the lung in a porcine lung model. Ablation was performed using the standard protocol of an FDA-approved NanoKnife System. An acute but recoverable bronchial injury was found. The morphological changes were comprehensively described by a CT follow-up, gross anatomy, pathological changes on an H&E stain and TEM. The indicators of myocardial enzymes and white blood cell counts showed an obvious increase within 2 days of ablation and all indicators had returned to preoperative levels within 14 days. Pathological examinations showed injured vascular epithelium cells in the ablation zone, however the structures of the bronchioli and vascular extracellular matrix were preserved. The epithelial cells were regenerated by 14 days post-ablation. No severe complications were observed and all of the experimental animals survived until the end-point of the study. These findings indicate the safety of CT-guided IRE ablation in a porcine lung. In the animal lung model, the ablation zone was confirmed using CT with serrated edges of high density in CT scanning images immediately after ablation. The density of the ablation was significantly increased after 24 h, indicating the density of soft tissues. Similar observations were reported by Deodhar et al. [21]; in this study, complete ablation was successfully achieved in all of the experimental animals, with no severe treatment-related complications, such as arrhythmia or blood pneumothorax. Minor needle-tract bleeding was observed in two cases (28.6%), and symptoms of mild pneumothorax were observed in one case (14.3%), which was comparable with the incidences of hemorrhage and pneumothorax that occurred during pulmonary puncture biopsy, as reported in the literature [23]. However, the complications could be controlled with an improved, smaller probe and navigation device. All of the experimental animals achieved a complete recovery 0.5 to 2 h post-IRE ablation. The key procedures include effective muscle relaxants and temperature maintenance during anesthesia. Precise probe placement and full muscle relaxants are critical. Enzymes such as AST, LDH, CKMB, and HBD, which are normally present in cardiac tissue, are released as a result of acute myocardial damage. In this study, the levels of myocardial enzymes were measured before and after IRE ablation by nephelometry. The levels of these indicators of myocardial damage had increased significantly and the white blood cell count was elevated dramatically at 2 h post IRE ablation, while further laboratory follow-up found that these levels were gradually reduced 2 days after IRE ablation and they eventually recovered 14 days post-ablation. These transient increases of myocardial enzymes indicate that IRE near the heart can cause acute but recoverable myocardial damage. Therefore, a minimum distance should be kept of 2 cm between the ablation probe and the heart [24]. Dupuy et al. observed chronic inflammatory changes in the blood vessels and airway between 2 and 4 weeks after IRE ablation of lung tissues, although no thrombus or structural collapse was found. Moreover, the reactive regeneration of alveolar cells and metapla-

sia of airway epithelial cells was also found [20]. In our study, the serial pathological examinations of cell death in the alveoli, bronchioles, and the vascular epithelium were found in the ablation zone. However, the skeletal structures of bronchioli and the extracellular matrix of the vasculature were preserved. At 14 days after ablation, endothelial cell regeneration was observed and the bronchioles and small blood vessels were filled with cell debris, collagen, and hemoglobin. These findings indicate that the structure of the bronchioles and the small blood vessels remain intact after IRE ablation. The injured bronchial endothelial cells gradually regenerate. Furthermore, although the inner lumen may be partially or completely occluded in the short term, the recanalization can be achieved gradually over time. This remains to be confirmed in a long-term follow-up. In conclusion, the results of this study indicate that IRE ablation is feasible for use in the lungs. Further studies should be designed to provide radiographic evidence with a longer follow-up.

Acknowledgements

All authors thank Professor Bill Thompson from English Language Center, Old Dominion University in Norfolk, VA, U.S.A who proofread the manuscript. This work was supported by grants from the National Natural Science Foundation of China [grant numbers 81371658, 81572307, 81572954, 81600506]; Zhejiang Provincial Natural Science Foundation of China under Grant No. LZ18H180001; National S&T Major Project (No. 2018ZX10301201); Basic Health Appropriate Technology for the Transformation of Major Projects during the 12th Five-Year Plan Period of Zhejiang Province [grant numbers 2013T301-15]; Major Project of Medical and Health Technology Development Program in Zhejiang Province [grant numbers 7211902]; National Key Basic Research Development Program (973 Program) [grant numbers 2013-CB531403]; Medical Health Fund of Zhejiang Province (grant No. 2013KYB097), Science and Technology Major Project of Zhejiang Province [grant numbers 2014C13G2010059]; Traditional Chinese Medicine Science Research Fund Project of Zhejiang Province (grant numbers 2017ZA079); and China Postdoctoral Science Foundation (grant numbers 2017464).

Disclosure of conflict of interest

None.

Address correspondence to: Wei-Lin Wang, Hepatobiliary and Pancreatic Interventional Treatment Center, Division of Hepatobiliary and Pancreatic Surgery, The First Affiliated Hospital, School of Medicine, Zhejiang University, Hangzhou 310003, China. E-mail: wam@zju.edu.cn

References

[1] Little MW, Chung D, Boardman P, Gleeson FV and Anderson EM. Microwave ablation of pulmonary malignancies using a novel high-energy antenna system. Cardiovasc Intervent Radiol 2013; 36: 460-465.

[2] Yan TD, King J, Sjarif A, Glenn D, Steinke K, Morris DL. Percutaneous radiofrequency ablation of pulmonary metastases from colorectal carcinoma: prognostic determinants for survival. Ann Surg Oncol 2006; 13: 1529-1537.

[3] Riccardo L, Crocetti L, Roberto C, Robert S, Derek G, Daniele R, Thomas H, Alice RG, Andrea F, Marcello A, Carlo B, Alfredo M. Response to radiofrequency ablation of pulmonary tumours: a prospective, intention-to-treat, multicentre clinical trial (the RAPTURE study). Lancet Oncol 2008; 9: 621-628.

[4] Vogl TJ, Naguib NN, Lehnert T and Nour-Eldin NE. Radiofrequency, microwave and laser ablation of pulmonary neoplasms: clinical studies and technical considerations--review article. Eur J Radiol 2011; 77: 346-357.

[5] Wang H, Littrup PJ, Duan Y, Zhang Y, Feng H, Nie Z. Thoracic masses treated with percutaneous cryotherapy: initial experience with more than 200 procedures. Radiology 2005; 235: 289-298.

[6] Savic LJ, Chapiro J, Hamm B, Gebauer B and Collettini F. Irreversible electroporation in interventional oncology: where we stand and where we go. Rofo 2016; 188: 735-45.

[7] Wendler JJ, Pech M, Blaschke S, Porsch M, Janitzky A, Ulrich M, Dudech O, Ricke J, Liehr UB. Angiography in the isolated perfused kidney: radiological evaluation of vascular protection in tissue ablation by nonthermal irreversible electroporation. Cardiovasc Intervent Radiol 2012; 35: 383-390.

[8] Wendler JJ, Pech M, Porsch M, Janitzky A, Fishchbach F, Buhtz P, Buhtz P, Vogler K, Huhne S, Boruchi K, Strang C, Mahnkopf D, Ricke J, Liehr UB. Urinary tract effects after multifocal nonthermal irreversible electroporation of the kidney: acute and chronic monitoring by magnetic resonance imaging, intravenous urogra-

phy and urinary cytology. Cardiovasc Intervent Radiol 2012; 35: 921-926.
[9] Wendler JJ, Porsch M, Huhne S, Baumunk D, Buhtz P, Fischbach F, Pech M, Mahnkopf D, Kropf S, Roessner A, Ricke J, Schostak M, Liehr UB. Short- and mid-term effects of irreversible electroporation on normal renal tissue: an animal model. Cardiovasc Intervent Radiol 2013; 36: 512-520.
[10] Golberg A, Bruinsma BG, Uygun BE and Yarmush ML. Tissue heterogeneity in structure and conductivity contribute to cell survival during irreversible electroporation ablation by "electric field sinks". Sci Rep 2015; 5: 84-85.
[11] Narayanan G, Froud T, Suthar R and Barbery K. Irreversible electroporation of hepatic malignancy. Semin Intervent Radiol 2013; 30: 67-73.
[12] Scheffer HJ, Nielsen K, van Tilborg AA, Vieveen JM, Bouwman RA, Kazemier G, Niessen HW, Meijer S, van Kuijk C, van den Tol MP, Meijerink MR. Ablation of colorectal liver metastases by irreversible electroporation: results of the COLDFIRE-I ablate-and-resect study. Eur Radiol 2014; 24: 2467-2475.
[13] Thomson KR, Cheung W, Elis SJ, Federman D, Kavnoudias H, Loader-Oliver D, Roberts S, Evans P, Ball C, Haydon A. Investigation of the safety of irreversible electroporation in humans. J Vasc Interv Radiol 2011; 22: 611-621.
[14] Dunki-Jacobs EM, Philips P and Martin RC 2nd. Evaluation of resistance as a measure of successful tumor ablation during irreversible electroporation of the pancreas. J Am Coll Surg 2014; 218: 179-187.
[15] Valerio M, Dickinson L, Ali A, Ramachandran N, Donaldson I, Freeman A, Ahmed HU, Emberton M. A prospective development study investigating focal irreversible electroporation in men with localised prostate cancer: Nanoknife Electroporation Ablation Trial (NEAT). Contemp Clin Trials 2014; 39: 57-65.
[16] Pech M, Janitzky A, Wendler JJ, Strang C, Blaschke S, Dudech O, Riche J, Liehr UB. Irreversible electroporation of renal cell carcinoma: a first-in-man phase I clinical study. Cardiovasc Intervent Radiol 2011; 34: 132-138.
[17] Ricke J, Jurgens JH, Deschamps F, Tselikas L, Uhde K, Kosiek O, De Baere T. Irreversible electroporation (IRE) fails to demonstrate efficacy in a prospective multicenter phase II trial on lung malignancies: the ALICE trial. Cardiovasc Intervent Radiol 2015; 38: 401-408.
[18] Usman M, Moore W, Talati R, Watkins K and Bilfinger TV. Irreversible electroporation of lung neoplasm: a case series. Med Sci Monit 2012; 18: CS43-47.
[19] Wendler JJ, Porsch M, Fischbach F, Pech M, Schostak M, Liehr UB. Letter to the editor concerning "irreversible electroporation (IRE) fails to demonstrate efficacy in a prospective multicenter phase II trial on lung malignancies: the ALICE trial" by Ricke et al. 2015 (doi:10.1007/s00270-014-1049-0). Cardiovasc Intervent Radiol 2015; 38: 1064-1065.
[20] Dupuy DE, Aswad B and Ng T. Irreversible electroporation in a Swine lung model. Cardiovasc Intervent Radiol 2011; 34: 391-395.
[21] Deodhar A, Monette S, Single GW Jr, Hamilton WC Jr, Thornton RH, Sofocleous CT, Maybody M, Solomon SB. Percutaneous irreversible electroporation lung ablation: preliminary results in a porcine model. Cardiovasc Intervent Radiol 2011; 34: 1278-1287.
[22] Li ZW, Xiao YY and Du JB. Feasibility study on the application of CT-guided NanoKnife in animal lung ablation. Chin J Interv Imaging Ther 2015; 12: 271-274.
[23] Yeow KM, Su IH, Pan KT, Tsay PK, Lui KW, Cheung YC, Chou AS. Risk factors of pneumothorax and bleeding: multivariate analysis of 660 CT-guided coaxial cutting needle lung biopsies. Chest 2004; 126: 748-754.
[24] Deodhar A, Dickfeld T, Single GW, Hamilton WC Jr, Thornton RH, Sofocleous CT, Maybody M, Gonen M, Rubinsky B, Solomon SB. Irreversible electroporation near the heart: ventricular arrhythmias can be prevented with ECG synchronization. AJR Am J Roentgenol 2011; 196: W330-335.
[25] Wendler JJ, Fischbach K, Riche J, Jurgens J, Fischbach F, Kollermann J, Porsch M, Baumunk D, Schostak M, Liehr UB, Pech M. Irreversible electroporation (IRE): standardization of terminology and reporting criteria for analysis and comparison. Pol J Radiol 2016; 81: 54-64.
[26] Belfiore MP, Ronza FM, Romano F, Ianniello GP, De Lucia G, Gallo C, Marsicano C, Di Gennaro TL, Belfiore G. Percutaneous CT-guided irreversible electroporation followed by chemotherapy as a novel neoadjuvant protocol in locally advanced pancreatic cancer: our preliminary experience. Int J Surg 2015; 21 Suppl 1: S34-39.